Phase transitions of hard disks in external periodic potentials: A Monte Carlo study

W. Strepp,[1] S. Sengupta,[2] and P. Nielaba[1]
[1]*Physics Department, University of Konstanz, Fach M 691, 78457 Konstanz, Germany*
[2]*S. N. Bose National Centre for Basic Sciences, Block JD, Sector III, Salt Lake, Calcutta 700098, India*
(Received 24 October 2000; published 26 March 2001)

The nature of freezing and melting transitions for a system of hard disks in a spatially periodic external potential is studied using extensive Monte Carlo simulations. Detailed finite size scaling analysis of various thermodynamic quantities like the order parameter, its cumulants, etc., are used to map the phase diagram of the system for various values of the density and the amplitude of the external potential. We find clear indication of a reentrant liquid phase over a significant region of the parameter space. Our simulations therefore show that the system of hard disks behaves in a fashion similar to charge-stabilized colloids that are known to undergo an initial freezing, followed by a remelting transition as the amplitude of the imposed, modulating field produced by crossed laser beams is steadily increased. Detailed analysis of our data shows several features consistent with a recent dislocation unbinding theory of laser induced melting.

DOI: 10.1103/PhysRevE.63.046106 PACS number(s): 64.60.−i

I. INTRODUCTION

The liquid-solid transition in systems of particles under the influence of external modulating potentials has recently attracted a fair amount of attention from experiments [1–7], theory [8,9], and computer simulations [10–13]. This is partly due to the fact that well-controlled, clean experiments can be performed using colloidal particles [14] confined between glass plates (producing essentially a two-dimensional system) and subjected to a spatially periodic electromagnetic field generated by interfering two, or more, crossed laser beams. One of the more surprising results of these studies, where a commensurate, one-dimensional, modulating potential is imposed, is the fact that there exist regions in the phase diagram over which one observes reentrant [4–6] freezing/melting behavior. As a function of the laser field intensity the system first freezes from a modulated liquid to a two-dimensional triangular solid—a further increase of the intensity confines the particles strongly within the troughs of the external potential, making the system quasi-one-dimensional, which increases fluctuations and leads to remelting.

Our present understanding of this curious phenomenon has come from early mean-field density functional [8] and more recent dislocation unbinding [9] calculations. The mean-field theories neglect fluctuations and therefore cannot explain reentrant behavior. The order of the transition is predicted to be first order for small laser field intensities, though for certain combinations of external potentials (which includes the specific geometry studied in the experiments and in this paper) the transition may become second order after going through a tricritical point. In general, though mean field theories are applicable in any dimension, the results are expected to be accurate only for higher dimensions and long ranged potentials. The validity of the predictions of such theories for the system under consideration is, therefore, in doubt.

A more recent theory [9] extends the dislocation unbinding mechanism for two-dimensional melting [22] for systems under external potentials. For a two-dimensional triangular solid subjected to an external one-dimensional modulating potential, the only dislocations involved are those that have their Burgers vectors parallel to the troughs of the potential. The system, therefore, maps onto an anisotropic, scalar Coulomb gas (or *XY* model) [9] in contrast to a *vector* Coulomb gas [22] for the pure two-dimensional melting problem. Once bound dislocation pairs are integrated out, the melting temperature is obtained as a function of the renormalized or ''effective'' elastic constants that depend on external parameters like the strength of the potential, temperature, and/or density. Though explicit calculations are possible only near the two extreme limits of zero and infinite field intensities, one can argue effectively that a reentrant melting transition is expected on general grounds quite independent of the detailed nature of the interaction potential for any two-dimensional system subject to such external potentials. The actual extent of this region could, of course, vary from system to system. In addition, these authors predict that the auto-correlation function of the Fourier components of the density (the Debye-Waller correlation function) decays algebraically in the solid phase at the transition with a universal exponent that depends only on the geometry and the magnitude of the reciprocal lattice vector.

Computer simulation results in this field have so far been inconclusive. Early simulations [10] involving colloidal particles interacting via the Derjaguin-Landau-Verwey-Overbeek potential [14] found a large reentrant region in apparent agreement with later experiments. On closer scrutiny, though, quantitative agreement between simulation and experiments on the same system (but with slightly different parameters) appears to be poor [6]. Subsequent simulations [11–13] have questioned the findings of the earlier computation and the calculated phase diagram does not show a significant reentrant liquid phase.

Motivated, in part, by this controversy, we have investigated the freezing/melting behavior of an unrelated system subjected to similar modulating external potentials. In this paper we have computed the phase behavior of a two-dimensional hard disk system in an external potential. The pure hard disk system is rather well studied [15–18] by now and the nature of the melting transition in the absence of

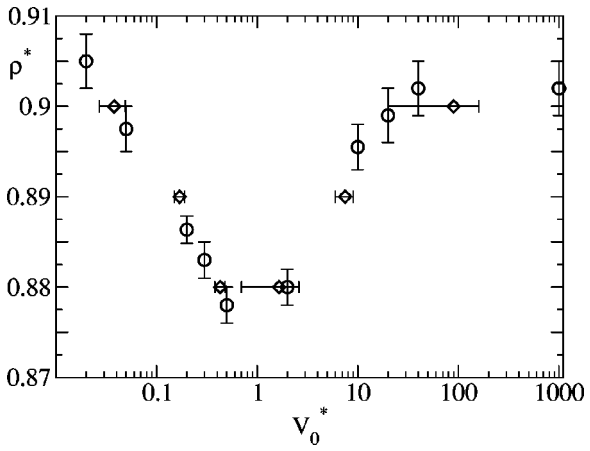

FIG. 1. Phase diagram in the ρ^*/V_0^* plane. Transition points for transitions from the solid to the modulated liquid have been obtained by the order parameter cumulant intersection method. In order to map the phase diagram we scanned in ρ^* for every V_0^*, starting from the high density (solid) region. The system size is $N=1024$.

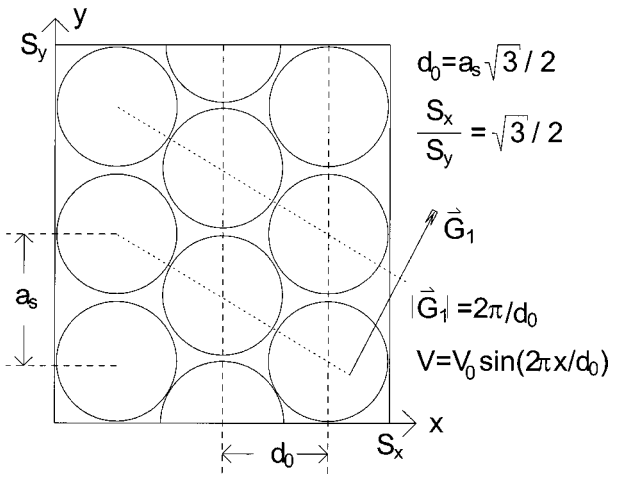

FIG. 2. Schematic picture of the system geometry showing the direction $\vec{G}_1$ along which crystalline order develops in the modulated liquid. The four vectors obtained by rotating $\vec{G}_1$ counterclockwise by 60° and/or reflecting about the origin are equivalent. The parameters d_0 and a_s are also shown. The size of the box is $S_x \times S_y$ and the modulating potential is V.

external potentials reasonably well explored. Also, there exist colloidal systems with hard interactions [14] so that, at least in principle, actual experiments using this system are possible. Finally, a hard disk simulation is relatively cheap to implement and one can make detailed studies of large systems without straining computational resources. The main outcome of our calculations, the phase diagram, is shown in Fig. 1. We have shown results from our simulation of a system of $N=1024$ hard disks (diameter σ) of density $0.86 < \rho^*(=\rho\sigma^2) < 0.91$ and the amplitude of the external potential $0 < V_0^*(=\beta V_0) < 1000$. Within our range of densities, one has a clear signature of a reentrant liquid phase showing that this phenomenon is indeed a general one as indicated in Ref. [9].

The rest of our paper is organized as follows. In Sec. II we specify the model and the simulation method including details of the finite size analysis used. In Sec. III we present our results for the order parameter and its cumulants with a discussion on finite size and hysteresis effects. We also present results for the specific heat, order parameter susceptiblity and correlation functions, which further illustrates the nature of the phase transitions in this system. In Sec. IV we discuss our work in relation to the existing literature on this subject, summarize and conclude.

II. MODEL AND METHOD

A. The model

We study a system of N hard disks of diameter σ in a two-dimensional box of size $S_x \times S_y$ ($S_x/S_y = \sqrt{3}/2$) interacting with the pair potential $\phi(r_{ij})$ between particles i and j with distance r_{ij},

$$\phi(r_{ij}) = \begin{cases} \infty, & r_{ij} \leqslant \sigma \\ 0, & r_{ij} > \sigma. \end{cases} \tag{1}$$

In addition, a particle with coordinates (x,y) is exposed to an external periodic potential of the form

$$V(x,y) = V_0 \sin(2\pi x/d_0). \tag{2}$$

The constant d_0 in Eq. (2) is chosen such that for a density $\rho = N/S_x S_y$, the modulation is commensurate to a triangular lattice of hard disks with nearest neighbor distance a_s, $d_0 = a_s\sqrt{3}/2$ (see Fig. 2). The only parameters that define our system are the reduced density $\rho\sigma^2 = \rho^*$ and the reduced potential strength $V_0/k_BT = V_0^*$, where k_B is the Boltzmann constant and T is the temperature.

B. The method

1. Numerical details

We perform Monte Carlo (MC) simulations [19,20] in the canonical (NVT) ensemble for the system with interactions given by Eqs. (1) and (2) for various values of V_0^* and ρ^*. Averages $\langle \cdot \rangle$ of observables have been obtained with the canonical measure. In order to obtain thermodynamic quantities for a range of system sizes, we have analyzed various quantities within subsystems as shown in Fig. 3. We have used $\langle \cdot \rangle_L$ to denote averages in subsystems. The subsystems are of size $L_x \times L_y$, where L_x and L_y are chosen as $L_y = L a_s$ and $L_x = L_y\sqrt{3}/2$ consistent with the geometry of the triangular lattice.

Most of the simulations described below have been done for $N=1024$ particles unless otherwise indicated. Phase transitions have been studied in most cases by starting in the ordered solid and reducing ρ^* for fixed V_0^*. Runs where the density ρ^* is increased were also performed in a few cases.

A typical simulation run with 4×10^7 Monte Carlo steps (MCS) (including 1.5×10^7 MCS for relaxation) took about 50 CPU hours on a PII/500 MHz PC. At high values of V_0^* in addition to ordinary (local) MC moves we also used ''through-moves,'' by which particle placements in neigh-

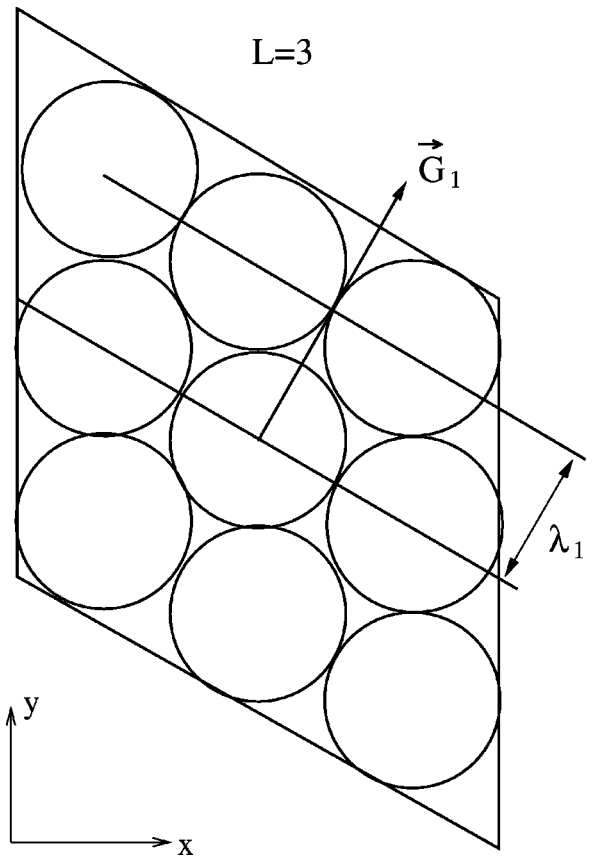

FIG. 3. Schematic picture showing sub-boxes of size L (here $L=3$) used in the finite size scaling analysis (see text).

boring troughs are tried. Besides producing faster equilibration, including such moves ensures that the formation of dislocations for large V_0^* and $\rho^* > \sqrt{3}/2$ ($d_0 < \sigma$) are not artificially hindered since particles can bypass each other—this is impossible with purely local MC moves.

To guarantee good equilibration and averaging, we simulated only systems up to $N=1600$ particles in the region of the phase boundary. Systems with $N=4096$ and $N=16\,384$ were used only once in Fig. 11, where the interesting region is clearly in the liquid phase and equilibration is much easier.

2. Order parameter

The nature of the fluid-solid phase transition in two dimensions has been a topic of controversy throughout the last 40 years [21–23,16,17,24,18]. It is well known that true long range positional order is absent in the infinitely large system due to low energy long wavelength excitations so that translational correlations decay algebraically. According to the dislocation unbinding mechanism [22,23], the two-dimensional solid (with quasi-long-ranged positional order) first melts into a ''hexatic'' phase with no positional order but with quasi long ranged orientational order signified by a nonzero bond orientational order parameter $\psi_6 = \Sigma \exp(-i6\theta)$ where θ is the angle of a bond and the sum is over all distinct bonds. A liquid, with no bond orientational order either ($\psi_6=0$) is produced by a second Kosterlitz-Thouless (KT) [22] transition from the hexatic.

In an external periodic field given by Eq. (2), however, the bond orientational order parameter is nonzero even in the fluid phase [9,12]. This is because for $V_0^* \neq 0$ we have now a ''modulated'' liquid, in which local hexagons consisting of the six nearest neighbors of a particle are automatically oriented by the external field. Thus $\langle \psi_6 \rangle$ is nonzero both in the (modulated) liquid and the crystalline phase and it cannot be used to study phase transitions in this system. The order parameters corresponding to a solid phase are the Fourier components of the (nonuniform) density $\rho(\vec{r})$ calculated at the reciprocal lattice points $\{\vec{G}\}$. This (infinite) set of numbers are all zero (for $\vec{G} \neq 0$) in a uniform liquid phase and nonzero in a solid. We restrict ourselves to the star consisting of the six smallest reciprocal lattice vectors of the two-dimensional triangular lattice. In the modulated liquid phase that is relevant to our system, the Fourier components corresponding to two out of these six vectors, viz., those in the direction perpendicular to the troughs of the external potential, are nonzero [8]. The other four components of this set consisting of those in the direction $\vec{G}_1$ (as defined for the ideal crystal in Fig. 2), and those equivalent to it by symmetry, are zero in the (modulated) liquid and nonzero in the solid (if there is true long range order). We therefore use the following order parameter:

$$\psi_{G_1} = \left| \sum_{j=1}^{N} \exp(-i\vec{G}_1 \cdot \vec{r}_j) \right|,$$

where $\vec{r}_j$ is the position vector of the jth particle. Note that though the order parameter $\langle \psi_{G_1} \rangle$ decays to zero with increasing system size in the 2D solid—quasi-long-ranged order—this decay, being weak, does not hinder us from distinguishing, in a finite system, a modulated liquid from the solid phase with positional order in the $\vec{G}_1$ direction.

3. Cumulants

We have determined phase transition points by the order parameter cumulant intersection method [25]. The fourth order cumulant U_L of the order parameter distribution is given by

$$U_L(V_0^*, \rho^*) = 1 - \frac{\langle \psi_{G_1}^4 \rangle_L}{3\langle \psi_{G_1}^2 \rangle_L^2}. \tag{3}$$

In the case of a continuous transition close to the transition point, the cumulant is only a function of the ratio of the system size $\approx L a_s$ and the correlation length ξ: $U_L(La_s/\xi)$. Since ξ diverges at the critical point the cumulants for different system sizes intersect in one point: $U_{L_1}(0) = U_{L_2}(0) = U^*$. Even for first order transitions these cumulants intersect [26] though the value U^* of U_L as the intersection is not universal any more. The intersection point can, therefore, be taken as the phase boundary regardless of the order of the transition. This is useful since the order of the melting tran-

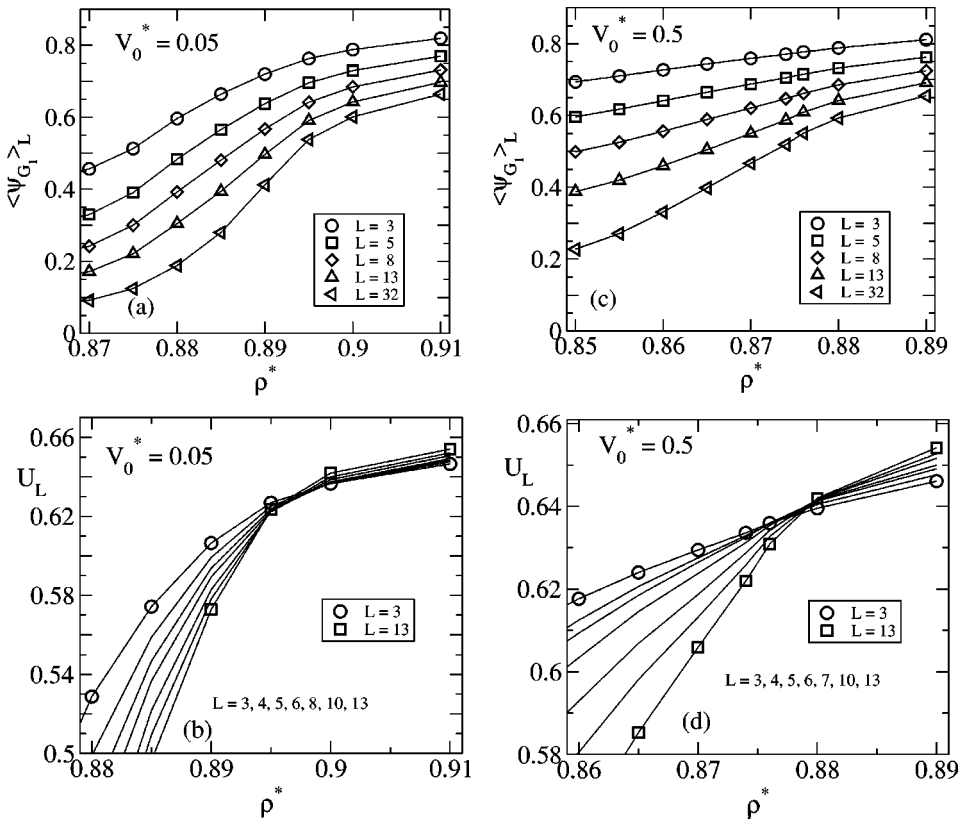

FIG. 4. Order parameter $\langle \psi_{G_1} \rangle_L$ [(a) and (c)] and order parameter cumulant U_L [(b) and (d)] versus ρ^* in subsystems of size L for reduced potential amplitudes $V_0^* = 0.05$ [(a) and (b)] and $V_0^* = 0.5$ [(c) and (d)], $N = 1024$. Unless otherwise stated, lines connecting data points in this and the rest of the figures are for visual guidance.

sition in 2D either in the absence [21–23,16,17,24,18] or with [8,10–13,9] external potentials is not unequivocally settled.

In order to map the phase diagram we systematically vary the system parameters V_0^* and ρ^* to detect order parameter cumulant intersection points that are then identified with the phase boundary. It should be noted that though the order parameter (defined for long range positional order) vanishes [22,23] with increasing system size in the crystalline phase, its cumulants are well defined and can be used to determine phase boundaries. For large L the cumulants approach the value 2/3 in the solid phase and 1/3 in the liquid [30] so that they are guaranteed to intersect. For very large V_0^* we do not find a unique point of intersection for U_L, instead the cumulants for various values of L collapse onto a single curve. In this case the onset of the collapse is taken as the ''intersection'' density. It is curious to note that this behavior is, in fact, typical of the anisotropic XY model [27]. In this case although the order parameter cumulants have an intersection point, the value of the cumulant at the intersection differs for various anisotropies and drifts towards a limiting value at zero anisotropy. The intersection ''point'' therefore changes to a ''line'' of intersections for different system sizes and for small anisotropies. In our system, for the large V_0^* we see similar behavior.

III. RESULTS AND DISCUSSION

A. Order parameter and cumulants

In Fig. 4 we present data for the average order parameter $\langle \psi_{G_1} \rangle$ and its cumulants as functions of the density for $V_0^* = 0.05$ and $V_0^* = 0.5$ calculated within various subsystems. In both cases $\langle \psi_{G_1} \rangle_L$ and U_L increase with ρ^* with a sharpening of the structures for increasing L. As discussed above, we observe that for any density increasing subsystem size L depresses $\langle \psi_{G_1} \rangle_L$. The cumulant U_L, on the other hand, approaches limiting values (2/3 for solid and 1/3 for liquid). The values of the cumulants are higher for larger L in the ordered (solid) phase and vice versa in the disordered (modulated liquid) phase thus resulting in an intersection point—the transition density.

In Fig. 5 we compare the density dependence of the average order parameter $\langle \psi_{G_1} \rangle$ (calculated over the entire sys-

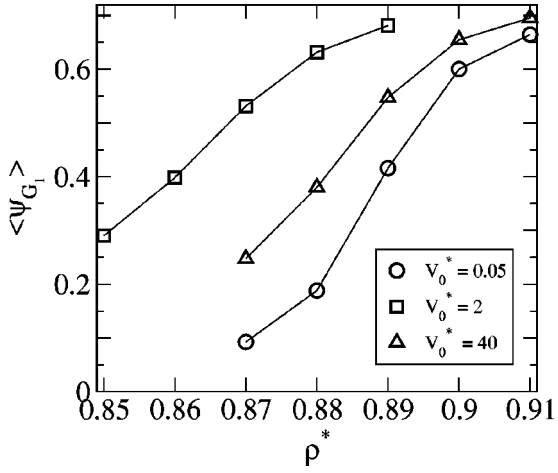

FIG. 5. Average order parameter $\langle \psi_{G_1} \rangle$ versus density for $V_0^* = 0.05$, 2, and 40, the system size is $N = 1024$.

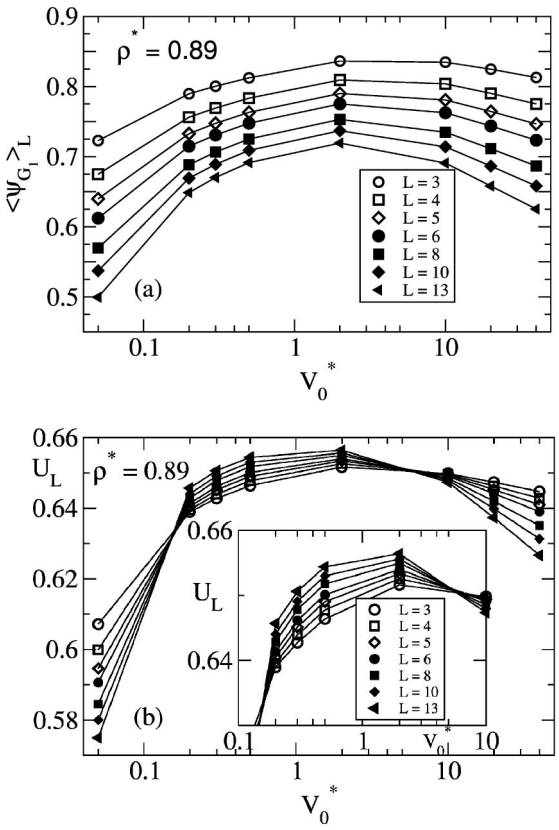

FIG. 6. Order parameter $\langle \psi_{G_1} \rangle_L$ (a) and order parameter cumulant U_L (b) versus V_0^* at a constant density $\rho^* = 0.89$ for different L, the system size is $N = 1024$.

tem) for different V_0^* and for the same system size ($N = 1024$). With increasing V_0^* the turning point in $\langle \psi_{G_1} \rangle (\rho^*)$ is shifted to lower densities and then for even larger V_0^* values to higher densities. This indicates, already, that the system prefers having smaller transition densities for intermediate values of V_0^* compared to smaller and higher V_0^* values—i.e., we have a reentrant transition.

In Fig. 6 we show a systematic study of $\langle \psi_{G_1} \rangle_L$ and U_L as a function of V_0^* at the density $\rho^* = 0.89$ for different L values. Maxima in the $\langle \psi_{G_1} \rangle_L$ and U_L curves are found near

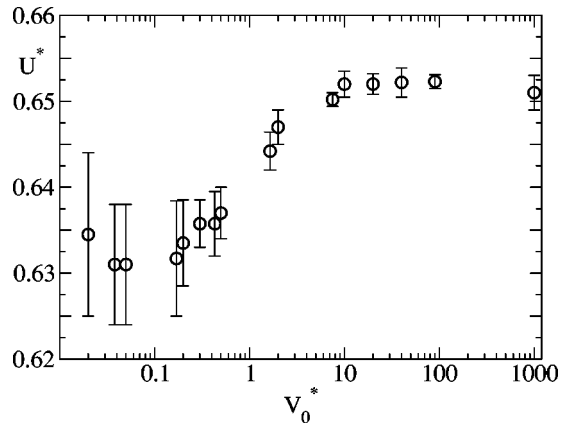

FIG. 8. Values U^* of the order parameter cumulants at the intersection points versus V_0^*. The shown data at the largest four values of V_0^* are taken at the onset of the cumulants curves merging (see text). The system size is $N = 1024$.

$V_0^* = 2$. Again we note that the $\langle \psi_{G_1} \rangle_L$ values decrease with increasing L [see Fig. 6(a)]. The cumulants U_L, on the other hand, increases with L for intermediate values of V_0^* (the ordered, solid phase) and decreases with L for either large or small V_0^* (the disordered, liquid phase) resulting in intersection points indicating two consecutive phase transitions [see Fig. 6(b)].

If V_0^* is increased to 20 the value of the cumulant at intersection U^* is shifted upwards, see Fig. 7(a). For very high V_0^* values the cumulant curves for different L merge on the high density side, see Fig. 7(b) (see discussion in Sec. II B 3). In Fig. 8 the cumulant intersection values are shown as a function of V_0^*, where for large V_0^* values the value at the onset of the merging is shown. We observe that U^* is not an universal number but, nevertheless, goes to a limiting value for large V_0^* [27].

In Fig. 9 we show $\langle \psi_{G_1} \rangle$ as a function of the density with $V_0^* = 0.5$ for different N values. The general features of $\langle \psi_{G_1} \rangle$ as discussed above is retained though there is a shift of the turning point to slightly higher densities with increasing N. The effect on the phase diagram is discussed in Sec. III C.

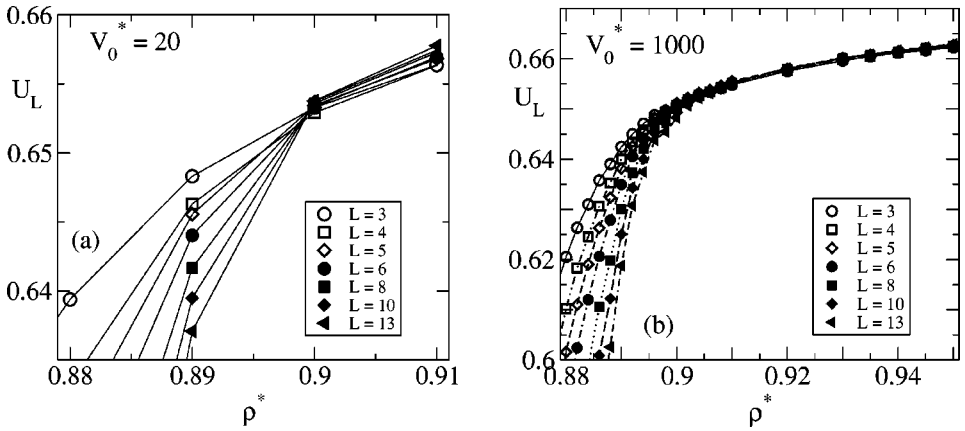

FIG. 7. Order parameter cumulants U_L versus ρ^* at constant $V_0^* = 20$ (a) and $V_0^* = 1000$ (b) for different L. The system size is $N = 1024$.

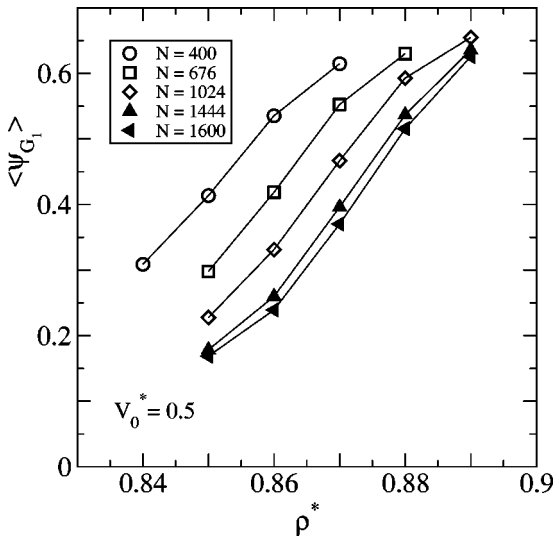

FIG. 9. Order parameter $\langle \psi_{G_1} \rangle$ versus density for different system sizes ($N=400,676,1024,1444,1600$) and $V_0^*=0.5$.

B. Susceptibility, specific heat, finite size effects, and hysteresis

In addition to $\langle \psi_{G_1} \rangle_L$ and U_L, we have computed the order parameter susceptibility χ_{G_1} and the specific heat for different system and subsystem sizes.

The order parameter susceptibility χ_{G_1} is defined as [30]

$$k_B T \chi_{G_1} = L^2 [\langle (\psi_{G_1})^2 \rangle - \langle \psi_{G_1} \rangle^2]. \tag{4}$$

In Fig. 10(a) we show χ_{G_1} as a function of ρ^* at $V_0^*=0.05$ for different L values. The increase of χ_{G_1} with increasing L, signals the presence of a phase transition in the density range where the transition has been found by cumulant intersection techniques ($\rho_t^* \approx 0.896$). In Fig. 10(b) χ_{G_1} is shown for the same system size ($N=1024$) and various V_0^* values. We note that the density of the χ_{G_1} maxima are the smallest for the intermediate value of V_0^*, which again show that for these V_0^* values the transition density is the lowest. Compared to the cumulant intersection values, χ_{G_1} maxima are located at slightly smaller densities (see also Sec. III C) that may be due to finite size effects, which often show the feature that phase transition points in finite systems

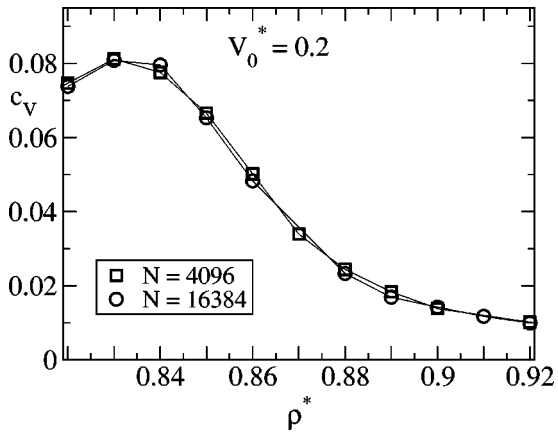

FIG. 11. Specific heat per particle versus density at constant $V_0^*=0.2$ and different system sizes ($N=4096,16384$).

are shifted to slightly different values depending on the observable under investigation. In particular, one expects (and we get) a shift towards parameter values in the disordered region (here a liquid, i.e., low densities) for the order parameter and the susceptibility as compared to the cumulant intersection parameters.

We have also calculated the specific heat C_V (Fig. 11) as a function of the density for $V_0^*=0.2$ with $N=4096$ and $N=16\,384$. For a second order transition, the maximum of the specific heat scales with the system size as $C_V^{max} \sim L^{\alpha/\nu}$ where α and ν are critical exponents. For a first order transition, on the other hand, $C_V^{max} \sim L^d$, where d is the dimensionality ($=2$ in our case). We, however, do not see any of this behavior. In contrast, the specific heat is relatively featureless. Although it shows a peak, surprisingly, the height of this peak is almost insensitive to system size. This is a strong indication that the phase transition we observe is unconventional and is KT-like [22,9]. Further, as expected for such transitions, the maximum does not lie at the density where the cumulants intersect and it would be incorrect to identify specific heat maxima with the phase boundary (see discussion in Sec. IV).

In order to study the effect of the path taken through the parameter space on the location of the cumulant intersection densities, we compared U_L as a function of the density for $V_0^*=0.5$ as obtained from two runs. In Fig. 4(d) we have already presented the data for a run where the density was

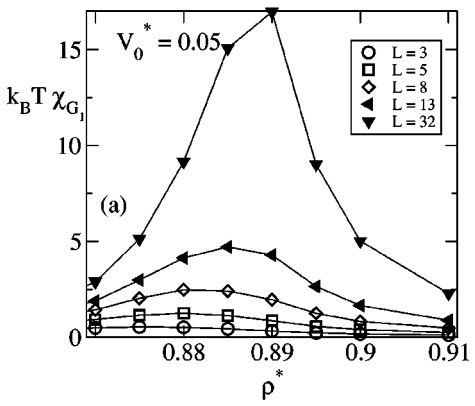

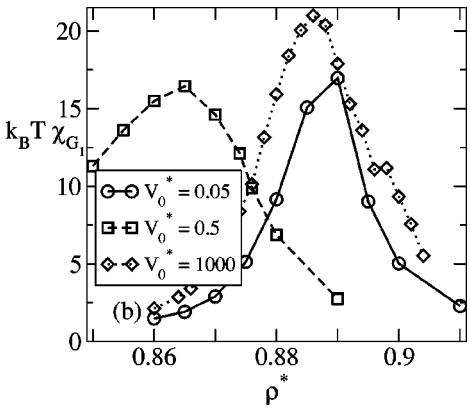

FIG. 10. Order parameter susceptibilities versus density for (a) constant $V_0^*=0.05$ and different L values, $N=1024$, (b) full system size ($N=1024$) and different V_0^* values.

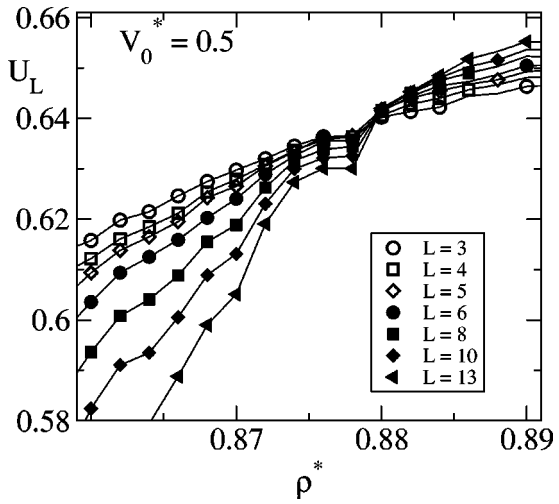

FIG. 12. Order parameter cumulant U_L versus density at constant $V_0^*=0.5$ and different L, $N=1024$. Values are obtained by successively compressing the system from one density to the next higher density. For a corresponding picture obtained by successively expanding the system see Fig. 4(d).

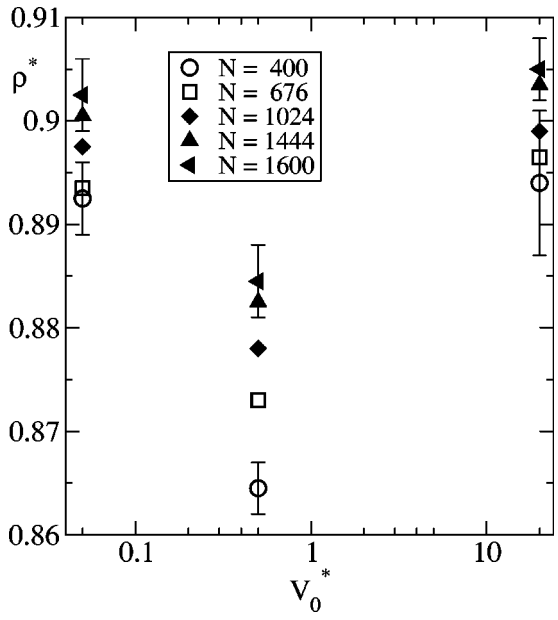

FIG. 13. Phase diagram in the ρ^*/V_0^* plane for different system sizes ($N=400,676,1024,1444,1600$).

decreased systematically. In Fig. 12 we present data for a second run where the density was *increased* instead. We find negligibly small hysteresis effects on the cumulants as well as on the value of intersection density. This shows that the transition points are not affected much by the path through the parameter space.

C. The phase diagram

We have obtained the phase diagram of the system for $0.86<\rho^*<0.91$ and $0<V_0^*<1000$. For each density and V_0^* value we computed cumulants U_L for a range of subsystem sizes L and located intersection points that we identify with the phase boundary. The resulting locus of the transition points is shown in the phase diagram, see Fig. 1. At very small values of V_0^*, we find good agreement of our transition densities with the melting densities ($\rho_m \approx 0.91$) known from literature [17] on the pure hard disk solid ($V_0^*=0$). The values of the transition density initially drop and subsequently rise as V_0^* increases. The minimum transition density is found for $V_0^* \approx 1-2$. These transition points separate a high density solid from a low density modulated liquid. Thus, at a properly chosen density, we observe an initial freezing transition followed by a reentrant melting at a higher V_0^* value. Such an effect had been found earlier in experiments on colloidal systems in an external laser field [4–6].

In order to quantify finite size effects on the phase diagram, we have computed the transition points for different system sizes. The resulting phase diagrams are shown in Fig. 13. We note that due to residual finite size effects with increasing system size all transition points are slightly shifted to higher densities, the structure of the phase diagram with a pronounced minimum at intermediate values of V_0^* is not affected by this shift.

D. Correlation functions

The Debye-Waller correlation function is defined as follows:

$$C_{\vec{G}_1}(\vec{R}) = |\langle e^{i\vec{G}_1[\vec{u}(\vec{R})-\vec{u}(0)]}\rangle|,$$

where $\vec{R}$ points to the elementary cell of the ideal lattice, and $\vec{u}(\vec{R})$ is the deviation of the actual particle position from the ideal lattice: $\vec{r}=\vec{R}+\vec{u}(\vec{R})$. In this case we have chosen the direction of $\vec{R}$ to lie along the y axis (i.e., along the troughs of the potential).

We have also computed the spatial correlation function $g(y)$, which is the pair correlation function in the y direction. We compute it in the following way: for a particle i, $g(y)dy \propto$ number of particles j for which $|y_i-y_j| \in [y, y+dy]$ and $|x_i-x_j|<d_0/2$, normalized so that $g(y)\to 1$ as $y \to \infty$.

These correlation functions are plotted in Fig. 14 as functions of y. The Debye-Waller correlation function $C_{G_1}(y)$ and the correlation function $g(y)$ along the potential valley are compared in Fig. 14(a) at a density just below the transition. We see that the decay of the maxima of $g(y)$ as function of y is similar to the decay in $C_{G_1}(y)$. The decay of $C_{G_1}(y)$ is analyzed in more detail in Fig. 14(b) for parameter values in the liquid and in the solid phase. In the liquid phase the decay is exponential while in the solid region it is algebraic: $C_{G_1}(y) \sim y^{-\eta_{G_1}}$. Taking the data points in the crystal that are closest to the phase boundary for each V_0^*, we get η_{G_1} in the range of $0.20,\ldots,0.27$. The exponent η_{G_1} is predicted [9] to be universal at the transition and equal to 1/4 for our geometry, so this value is consistent with our numerical results.

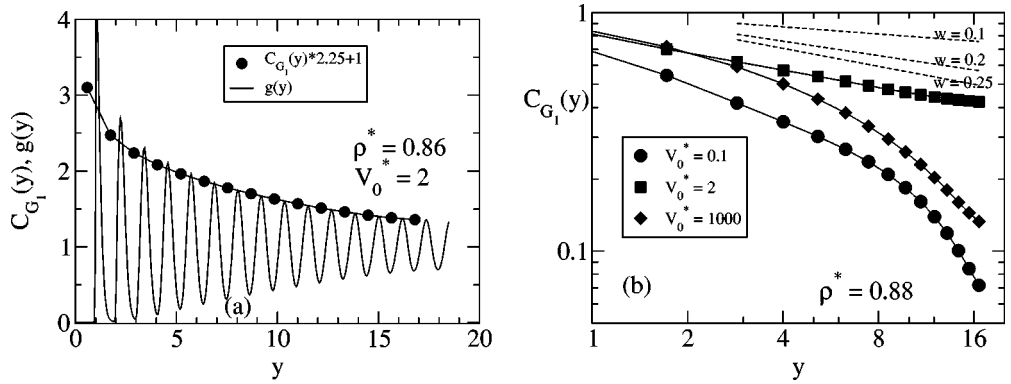

FIG. 14. Debye-Waller $[C_{G_1}(y)]$ correlation and pair distribution $[g(y)]$ functions as functions of y parallel to the potential minima for fixed $\rho^*=0.86$ and $V_0^*=2$ (a) and Debye-Waller correlation function versus y for fixed $\rho^*=0.88$ and different $V_0^*=0.1,2,1000$ (b). Lines in the upper right corner of (b) show the functions $f(y)=y^{-w}$ $(w=0.1,0.2,0.25)$ for comparison. The system size is $N=1024$.

E. Scaling behavior

We next try to determine the order of the phase transitions encountered in this system for various values of V_0^*. In order to investigate this issue we studied the scaling behavior of the order parameter, susceptibility, and the order parameter cumulant near the phase boundary for a small (0.5) and a large (1000) V_0^*. From finite size scaling theory (for an overview see Ref. [20]) we expect these quantities to scale as [28]

$$\langle \psi_{G_1} \rangle_L L^b \sim f(L/\xi), \tag{5}$$

$$\chi_L k_B T L^{-c} \sim g(L/\xi), \tag{6}$$

$$U_L \sim h(L/\xi). \tag{7}$$

Here $b=\beta/\nu$, $c=\gamma/\nu$ (for critical scaling), and f,g,h are scaling functions. The correlation length ξ diverges as $\xi \propto (1-\rho/\rho_c)^{-\nu}$ for an ordinary critical point, while for a KT transition we have an essential singularity and $\xi \propto \exp[a(1-\rho/\rho_c)^{-\tilde{\nu}}]$.

According to general arguments given in Ref. [9], we expect that for a finite lattice, the identification of the properties of our system with those of the anisotropic XY model should improve with increasing V_0^*. Indeed, for large V_0^*, scaling according to the KT theory seems to be supported by our data. In Fig. 15 we have plotted the left-hand sides of Eqs. (7) and (6) versus L/ξ for $V_0^*=1000$, where data points for $0.86 \leqslant \rho^* \leqslant 0.898$ have been considered and $\rho_c^*=0.902$, obtained by cumulant intersection. In order not to introduce an unwarranted bias, we have separately considered (a) ordinary critical scaling and (b) a KT scaling forms and adjusted the values of the parameters until we obtained collapse of our data onto a single curve determined by a least square estimator (see Table I). Though good collapse of our data is observed both in (a) and (b), the numerical values for $\tilde{\nu}$, $\eta=2b$, and $c=2-\eta$ for KT scaling $(b\approx 0.138, c\approx 1.70, \tilde{\nu}\approx 0.44)$ are close to the predicted values [9] $(b=\eta/2=1/8, c=1.75, \tilde{\nu}=0.5)$.

The situation is less straightforward for $V_0^*=0.5$. The critical parameters were obtained in this case for densities $0.85 \leqslant \rho^* \leqslant 0.876$, with $\rho_c^*=0.878$. In Fig. 16(a) the data collapse looks slightly better than in Fig. 16(b), such that relying on this data alone one may conclude that KT scaling in

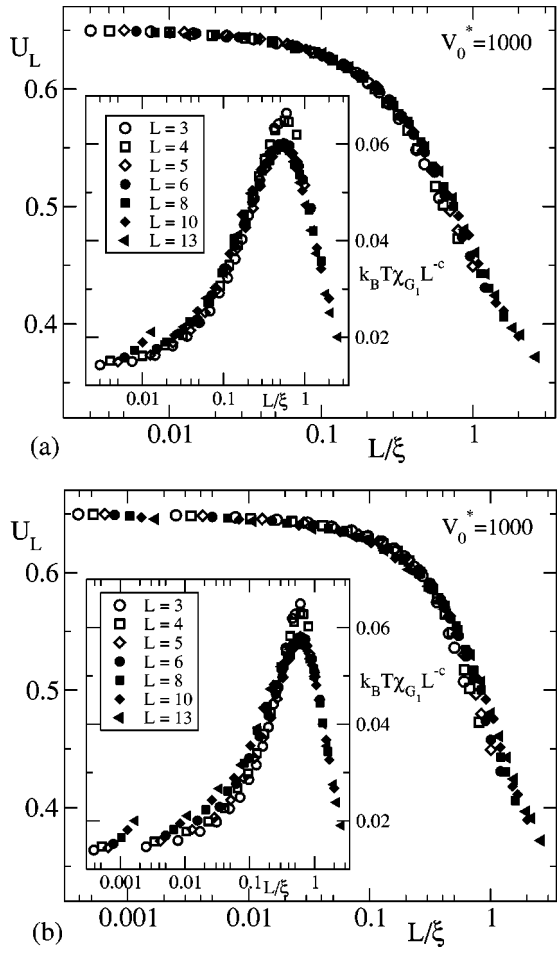

FIG. 15. Scaling plots for the order parameter cumulant and the susceptibility (inset) for $V_0^*=1000$ assuming (a) critical and (b) KT scaling. The system size is $N=1024$, for ξ we have used the expressions given after Eq. (7).

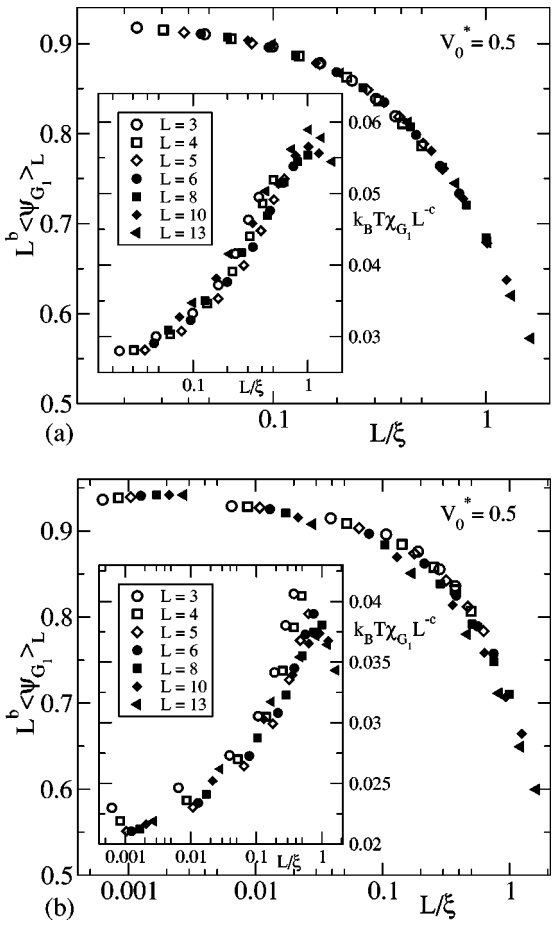

FIG. 16. Scaling plots for the order parameter and the susceptibility (inset) for $V_0^*=0.5$ assuming (a) critical and (b) KT scaling. The system size is $N=1024$, for ξ we have used the expressions given after Eq. (7).

this region of the phase diagram seems less likely. It must be kept in mind though that for small values of V_0^* in a finite system, the analysis of the data would be complicated by crossover effects. Strictly for $V_0=0$ we do not have a correspondence with the anisotropic XY model but rather with a *vector* Coulomb gas [22] with a different set of exponents. Our results for the numerical values of the parameters are summarized in Table I.

In summary, from the scaling analysis in Figs. 16 and 15 a KT scenario at least for large V_0^* values seems likely. This is supported by the behavior of the cumulants as well (see Sec. III A). A more precise classification of the phase transitions with the present data and system sizes is not easy. This topic is left for future work, in particular we plan to compute the elastic properties of the system by a method recently developed for the hard disk system [18,24] and to test the KT predictions [9].

IV. SUMMARY AND CONCLUSION

In summary, we have calculated the phase diagram of a two-dimensional system of hard disks in an external sinusoidal potential. We found freezing followed by reentrant melting transitions over a significant region of the phase diagram in tune with previous experiments on colloids [4–6] and with the expectations of a recent dislocation unbinding theory [9]. One of the main features of our calculation is the method used to locate phase boundaries. In contrast to earlier simulations [10–13] that used either the jump of the order parameter, or specific heat maxima to locate the phase transition, we have used the more reliable cumulant intersection method. It must be noted that the specific heat in this system does not show a strong peak at the phase transition density so that its use may lead to confusing results. This, in our opinion, may be the reason for part of the controversy in this field. It is possible that earlier simulations that used smaller systems and no systematic finite size analysis may have overlooked this feature of C_V, which becomes apparent only in computations involving large system sizes. We have shown that finite size scaling of the order parameter cumulants as obtained from subsystem or sub-block analysis, on the other hand, yields an accurate phase diagram.

What is the order of the phase transition? We know that [16–18] for the pure hard disk system in two dimensions this question is quite difficult to answer and our present understanding [18] is that hard disks in two dimensions show a KT transition [22]. This transition, however, lies very close (in an appropriately expanded parameter space) to a first order boundary so that crossover effects may be significant. The present system has an imposed external periodic potential that stabilizes the hexatic phase [9] and an (anisotropic) KT transition [9] is expected. Our results show several features that suggest that this is, perhaps, what we have. Though we have discussed these observations in the rest of the paper, we list them below for clarity.

The behavior of the value of the cumulants at intersection U^* is similar to an earlier work [27] on the anisotropic XY system that shows a KT transition.

The specific heat is relatively featureless and does not scale with system size in a fashion expected of a true first order or conventional continuous transition.

The decay of the correlation functions is similar to what is predicted [9] for an anisotropic scalar Coulomb gas.

For large V_0^* values the scaling of the order parameter, the susceptibility, and the cumulant may be described by the KT theory.

TABLE I. Parameters in the scaling plots (Figs. 16 and 15) for $V_0^*=0.5$ and $V_0^*=1000$. The first three parameter columns are for critical scaling, the last four for KT scaling.

V_0^*	b	c	ν	b	c	$\tilde{\nu}$	a
1000	0.13(1)	1.68(5)	2.25(25)	0.138(8)	1.70(5)	0.44(3)	1.05(25)
0.5	0.152(5)	1.65(6)	1.06(13)	0.170(12)	1.83(4)	0.38(10)	1.0(2)

Of course, in order to resolve this issue unambiguously, yet larger simulations are required. Also, we need to compute elastic properties [24,18] of this system in order to compare directly with the results of Ref. [9]. Work along these lines is in progress.

Before we end, we would like to point out that after completion of this work and prior to the submission of this manuscript we received a preprint [29] where the same system as ours has been studied using simulations. The phase diagram obtained by these authors is similar to ours (thus confirming and corroborating our results), though there exist some quantitative differences. These differences may be attributed to the absence of systematic finite size scaling in the latter work.

ACKNOWLEDGMENTS

We are grateful for many illuminating discussions with C. Bechinger and K. Binder. One of us (S.S.) thanks the Alexander von Humboldt Foundation for financial support. Support by the SFB 513 and granting of computer time from the NIC and the HLRS is gratefully acknowledged.

[1] N.A. Clark, B.J. Ackerson, and A.J. Hurd, Phys. Rev. Lett. **50**, 1459 (1983).
[2] A. Chowdhury, B.J. Ackerson, and N.A. Clark, Phys. Rev. Lett. **55**, 833 (1985).
[3] K. Loudiyi and B.J. Ackerson, Physica A **184**, 1 (1992); **184**, 26 (1992).
[4] Q.-H. Wei, C. Bechinger, D. Rudhardt, and P. Leiderer, Phys. Rev. Lett. **81**, 2606 (1998).
[5] C. Bechinger, Q.H. Wei, and P. Leiderer, J. Phys.: Condens. Matter **12**, A425 (2000).
[6] C. Bechinger, M. Brunner, and P. Leiderer, Phys. Rev. Lett. **86**, 930 (2000).
[7] K. Zahn, R. Lenke, and G. Maret, Phys. Rev. Lett. **82**, 2721 (1999).
[8] J. Chakrabarti, H.R. Krishnamurthy, and A.K. Sood, Phys. Rev. Lett. **73**, 2923 (1994).
[9] E. Frey, D.R. Nelson, and L. Radzihovsky, Phys. Rev. Lett. **83**, 2977 (1999).
[10] J. Chakrabarti, H.R. Krishnamurthy, A.K. Sood, and S. Sengupta, Phys. Rev. Lett. **75**, 2232 (1995).
[11] C. Das and H.R. Krishnamurthy, Phys. Rev. B **58**, R5889 (1998).
[12] C. Das, A.K. Sood, and H.R. Krishnamurthy, Physica A **270**, 237 (1999).
[13] C. Das, A. K. Sood, and H. R. Krishnamurthy (unpublished).
[14] For an introduction to phase transitions in colloids see, A.K. Sood, in *Solid State Physics*, edited by E. Ehrenfest and D. Turnbull (Academic Press, New York, 1991), Vol. 45, p. 1; P.N. Pusey, in *Liquids, Freezing and the Glass Transition*, edited by J.P. Hansen and J. Zinn-Justin (North-Holland, Amsterdam, 1991).
[15] K.W. Wojciechowski and A.C. Brańka, Phys. Lett. **134A**, 314 (1988).
[16] H. Weber, D. Marx, and K. Binder, Phys. Rev. B **51**, 14 636 (1995); H. Weber and D. Marx, Europhys. Lett. **27**, 593 (1994).
[17] A. Jaster, Phys. Rev. E **59**, 2594 (1999).
[18] S. Sengupta, P. Nielaba, and K. Binder, Phys. Rev. E **61**, 6294 (2000).
[19] N. Metropolis, A.W. Rosenbluth, M.N. Rosenbluth, A.H. Teller, and E. Teller, J. Chem. Phys. **21**, 1087 (1953).
[20] D. P. Landau, K. Binder, *A Guide to Monte Carlo Simulations in Statistical Physics* (Cambridge University Press, Cambridge, 2000).
[21] B.J. Alder and T.E. Wainwright, Phys. Rev. **127**, 359 (1962).
[22] J.M. Kosterlitz and D.J. Thouless, J. Phys. C **6**, 1181 (1973); B.I. Halperin and D.R. Nelson, Phys. Rev. Lett. **41**, 121 (1978); D.R. Nelson and B.I. Halperin, Phys. Rev. B **19**, 2457 (1979); A.P. Young, *ibid.* **19**, 1855 (1979); K.J. Strandburg, Rev. Mod. Phys. **60**, 161 (1988); H. Kleinert, *Gauge Fields in Condensed Matter* (World Scientific, Singapore, 1989).
[23] K.J. Strandburg, Phys. Rev. B **34**, 3536 (1986).
[24] S. Sengupta, P. Nielaba, M. Rao, and K. Binder, Phys. Rev. E **61**, 1072 (2000).
[25] K. Binder, Z. Phys. B: Condens. Matter **43**, 119 (1981); Phys. Rev. Lett. **47**, 693 (1981).
[26] K. Vollmayr, J.D. Reger, M. Scheucher, and K. Binder, Z. Phys. B: Condens. Matter **91**, 113 (1993).
[27] D.P. Landau, J. Magn. Magn. Mater. **31-34**, 1115 (1983).
[28] D.P. Landau, Phys. Rev. B **27**, 5604 (1983).
[29] P. Chowdhury, A. K. Sood, and H. R. Krishnamurthy (unpublished).
[30] Since ψ_{G_1} is the absolute value of a two-dimensional quantity, we can assume the following probability distribution in the (modulated) liquid and $L \gg \xi$ [26]:

$$w(\psi_{G_1}) = \frac{\psi_{G_1} 2L^2}{k_B T \tilde{\chi}} \exp\left(\frac{-\psi_{G_1}^2 L^2}{k_B T \tilde{\chi}}\right),$$

which yields $U_L = 1/3$, $\langle \psi_{G_1}^2 \rangle = k_B T \tilde{\chi}/L^2$, and $\chi = \tilde{\chi}(1-\pi/4)$ for χ defined as in Eq. (4). Because ψ_6 is very similar in spirit, the same results apply for $w(\psi_6)$ in an isotropic liquid and $L \gg \xi$.